Determination of the localization times of electrons and holes in the HgS well in a CdS/HgS/CdS quantum dot–quantum well nanoparticle

Markus Braun,* Stephan Link, Clemens Burda,† and Mostafa El-Sayed‡
School of Chemistry and Biochemistry, LDL, Georgia Institute of Technology, Atlanta, Georgia 30332
(Received 1 July 2002; published 11 November 2002)

The femtosecond time-resolved electron-hole dynamics of the CdS/HgS/CdS quantum dot–quantum well system (QDQW) was investigated as a function of excitation energy. In the transient absorption spectra four bleach bands and a stimulated emission signal in the visible spectral range between 450 and 780 nm were resolved. By using an IR probe pulse at 4.7 μm a transient induced absorption due to intraband transitions was found. The decay and rise times of these signals were measured when the CdS core or the HgS well of the nanoparticles was excited by the pump pulse. After excitation within the HgS well the transient signals rise within the resolution of our pump pulse, while after core excitation slower rise times were measured. From the 1.5 ps rise time of the stimulated emission originating from the HgS well and the intraband hole IR absorption (150 fs) after excitation into the CdS core, the electron localization time (transfer time from the core to the well) is found to be 1.5 ps while that of the hole is ~150 fs. This large difference in the observed dynamics of the electron and hole in crossing the CdS/HgS interface is discussed.

DOI: 10.1103/PhysRevB.66.205312 PACS number(s): 73.23.−b

I. INTRODUCTION

In recent years the synthesis of semiconductor heterostructures has strongly improved. These materials are promising candidates for applications in lasers,[1–3] optoelectronics,[4,5] and telecommunication.[6,7] In addition, the approach to build such quantum well or quantum dot heterostructures with the epitaxial deposition techniques and microstructurization on substrates under ultrahigh vacuum (UHV) conditions, there is also much interest in the chemical approach to synthesize colloidal solutions of semiconductor nanocrystals with narrow size distributions.[8–10] Reliable synthetic routes were developed to control and vary the size and shape of these nanocrystals by simple wet-chemical methods by changing parameters such as pH, temperature, or concentration. The electronic and mechanical properties of these nanoparticles can be varied by their size and shape due to quantum confinement effects,[11,12] when the particle size is in the range or smaller than the excitonic Bohr radius of the semiconductor bulk material used.

In so-called core-shell systems such as CdSe/ZnS, where a semiconductor nanocrystal is surrounded by one or two layers of a semiconductor with a larger band gap, fluorescence quantum efficiencies of nearly 100% at room temperature were achieved.[13] The wavelength of the absorption and fluorescence of these heterostructures can be changed over a large spectral range by varying the size of the nanoparticles.[8] For these reasons nanoparticles are very interesting as tunable fluorescence emitters in light emitting devices (LED's)[14,15] and microscopy[16,17] applications.

Eychmüller, Mews, and co-workers showed for the first time[18,19] that quantum well structures could be synthesized by use of wet chemical methods. They developed a synthetic route for the synthesis of a quantum dot–quantum well (QDQW) nanoparticle using the semiconductor materials CdS (band gap at 2.5 eV) and HgS (band gap at 0.5 eV).[18,19] In this system a CdS nanocrystal core is surrounded by one, two, or three monoshells of HgS which is then capped with CdS. Several experimental[18–27] and theoretical[28–30] investigations of this system have shown that after optical excitation the electron and hole in this heterostructure localize in the HgS well. In particular, Yeh *et al.*[24] have shown that the luminescence of this system originates from the radiative recombination of the electron and hole inside the HgS after the localization of both charge carriers. Depending on the number of the HgS shells the electron and hole states (and therefore the optical allowed transitions) can be shifted so that the absorption spectrum of the heterostructure spans the visible range and the near IR regions.

In order to investigate the nonradiative relaxation dynamics of the charge carriers, we used pump-probe femtosecond transient spectroscopy to monitor the dependence of the bleach, the stimulated emission, and the induced intraband absorption signals of the QDQW system with monolayer HgS well after an electron-hole pair was excited in the CdS core, or directly in the HgS well states. Previously, we reported[31] on the dependence of the rise time of these different signals on excitation at 400 nm into the CdS core or excitation at 650 nm into the HgS well. A connection between the rise times and the localization times of the electron and hole in the HgS well was made. Here we present further results using excitation wavelengths of 266 and 580 nm as well as 400 and 650 nm and also discuss the recovery of the transient absorption signals after excitation away from 400 nm.

II. EXPERIMENTAL

A. Synthesis

The CdS/HgS/CdS nanoparticles were prepared according to Mews *et al.*[19] with minor changes. The synthesis route consists of five steps: (1) growing of the CdS core, (2) exchanging the Cd^{2+} ions of the outermost CdS layer of the core with Hg^{2+} ions to form the well layer, (3) capping the

HgS layer by a monolayer of CdS, (4) increasing the CdS clad layer, (5) capping the QDQW particles with an organic layer to prevent aggregation. The successful formation of the QDQW structure was verified by optical absorption and fluorescence measurements and transmission electron microscopy (TEM). The size of the QDQW nanoparticles was 6 nm.

(1) Growing of the CdS core (diameter 3.6 nm). In a 250 ml three-neck flask (with septum, gas-inlet system, and pH meter) 100 ml deionized water ($R \geqslant 18\ M\Omega$) was purged for 30 min with argon. Then 0.2 ml of 0.1 M hexametaphosphate as stabilizer and 0.2 ml of 0.1 M $Cd(ClO_4)_2$ were added under stirring. The pH value was adjusted to 8.0 with a few drops of a 0.1 M NaOH solution. Under vigorous stirring 0.6 ml H_2S gas was injected through the septum in the space above the Cd^{2+} solution with a gas-tight syringe. During the next 10 min the pH value dropped to 4.6 and the formerly colorless solution became yellow due to the formation of CdS nanoparticles. After readjusting the pH value to 7.0 with a few drops of 0.1 M NaOH the excess H_2S was removed by bubbling the colloidal solution with argon for 30 min.

(2) Epitaxial growth of a monolayer of HgS. The Cd^{2+} ions of the outermost CdS layer were replaced by Hg^{2+} ions by adding 10 ml of 0.001 M $Hg(ClO_4)_2$ aqueous solution at pH 7.0 to the colloidal CdS solution under stirring. Thereby the solution changed its color immediately to a light red and the pH value increased to 7.6. The pH value was brought to 7.0 by adding 0.1 M $HClO_4$. The amount of Cd^{2+} ions of one CdS monolayer remained in the colloidal solution.

(3) Capping the CdS/HgS particle by a monolayer of CdS. The free Cd^{2+} ions were used for the epitaxial growth of a monolayer of CdS in order to cap the CdS/HgS particles. Therefore 25 ml of aqueous 5×10^{-4} M H_2S solution was added drop by drop during 25 min to hinder nucleation. This changes the color of the colloid to a light brown. Then, the pH value was readjusted to 7.0 and the colloidal solution was purged with argon to remove the excess of H_2S.

(4) Growing the CdS clad of the CdS/HgS/CdS particle. 0.2 ml of a 0.1 M $Cd(ClO_4)_2$ aqueous solution were added to the colloid. This amount is sufficient to form two monolayers of CdS around the nanoparticle. 50 ml of aqueous 5×10^{-4} M H_2S solution was added drop by drop during 25 min, the pH value was readjusted to 7.0, and the colloidal solution purged with argon to remove excess H_2S.

(5) Organic capping of the QDQW nanoparticles. To prevent aggregation of the so prepared QDQW nanoparticles, the sodium ions in the solution were exchanged with tetrabutyl-ammonium ions in a twofold dialysis process.[23] Then 30 ml of the colloid was concentrated to 1 ml by vacuum evaporation at 45 °C. In order to prepare a film of the QDQW nanoparticles, a few drops of that highly concentrated colloid were brought on a CaF_2 substrate and dried in a vacuum chamber for 24 h. The absorption spectrum in the range between 400 nm and 2.5 μm (not shown here) revealed the absence of water, which is necessary to perform transient absorption measurement in the IR range. All measurements were carried out at room temperature. The absorption spectrum of the film was measured before and after irradiation and evidence for decomposition could be found.

B. Femtosecond transient absorption measurements

The laser system is described in detail elsewhere.[26] The 100-fs pulses (800 nm, 800 mW, 1 kHz) were generated and amplified with a Ti-sapphire laser system (Clark MXR CPA 1000). The oscillator was pumped by a Nd:YVO ring laser (Coherent Verdi) while the regenerative amplifier was pumped with a Nd:YAG laser: As pump pulse either the second (400 nm) and third harmonic (266 nm) of the fundamental wavelength or the second harmonic and the sum frequency light of the output of an optical parametric amplifier (OPA) (TOPAS) at 580 and 650 nm were used. The pump pulses pass an optical chopper at 500 Hz. A white light continuum (430 nm to 1 μm) generated from focusing a small part of the fundamental pulse at 800 nm on a 1 mm sapphire plate was used as visible probe pulse. The IR probe pulse at 4.7 μm was generated by difference frequency generation from the signal and idler waves from a second OPA (TOPAS).

The pump and probe pulses were overlapped in the sample and the probe beam coupled into fiber optics. The change of the probe pulse absorption with and without excitation by the pump pulse was measured as a function of the delay time. The delay time between the probe and pump pulse was varied by an optical delay line with a resolution of 21 fs. The time dependent bleach spectra were recorded by a system consisting of monochromator and nitrogen cooled CCD camera. Optical transients were recorded by a system consisting of a monochromator and photodiodes (Si PIN diodes for the visible range and a nitrogen cooled HgCdTe detector for the IR probe).

III. RESULTS

A. Steady-state absorption and fluorescence

In Fig. 1 (top), the room temperature steady state absorption spectra of the colloidal solutions at different stages of the synthesis process are shown. The CdS nanoparticles [spectrum (a)] show a weak excitonic feature at 465 nm. For the CdS/HgS structure [spectrum (b)] the absorption edge is redshifted to 600 nm and the CdS/HgS/CdS QDQW nanoparticles [spectrum (c)] have an absorption edge, which extends to 700 nm. After additional growing of the CdS clad of the QDQW nanoparticles the structure denoted as $CdS/HgS/\{CdS\}_3$ is synthesized. It is obvious that the absorption of this structure [spectrum (d)] is not noticeably redshifted compared to spectrum (c). This is because the HgS well thickness, which strongly determines the optical properties of the QDQW structure in this region has not changed by increasing the CdS clad. Nevertheless the absorption strength of the QDQW was increased. This can be explained by the assumption that after exchanging the Cd^{2+} ions on the surface by Hg^{2+} ions in order to grow the CdS/HgS structure the amount of Cd^{2+} ions remaining in solution is not sufficient to cap the increased surface of the nanoparticles to form a complete first monolayer of the CdS clad. The second de-

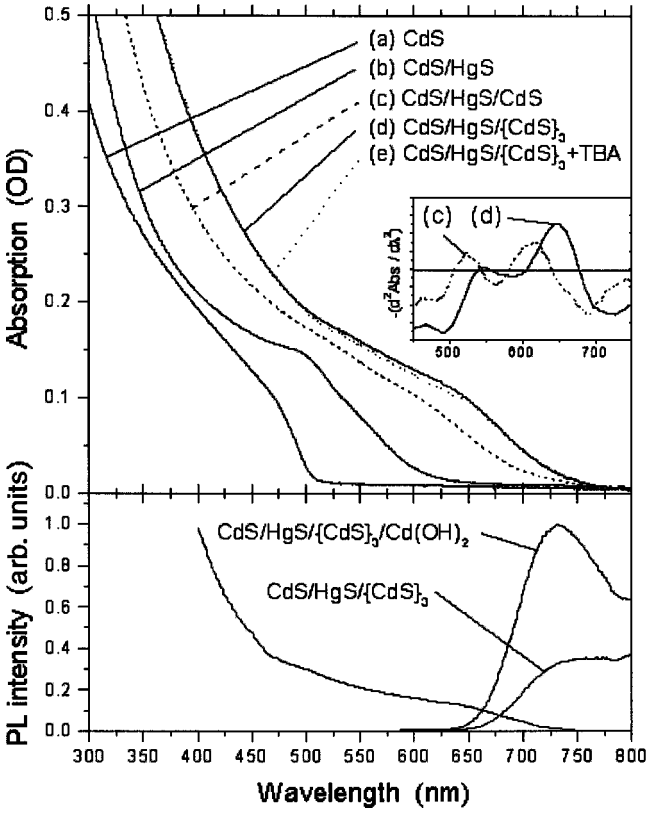

FIG. 1. (Top) Steady state absorption of the colloidal solutions at room temperature. The lowest energetic excitonic feature of the absorption shifts to the red in the series CdS nanoparticles (a) at 465 nm, CdS/HgS nanoparticles, (b) at 500 nm, QDQW nanoparticles CdS/HgS/CdS, (c) at 625 nm, and QDQW nanoparticles CdS/HgS/$\{CdS\}_3$, (d) at 640 nm. Changing the organic capping of the structure (d) by exchanging the sodium ions with tetra-butyl-ammonium ions does not influence the absorption of the QDQW (e). The inset shows the second derivative of the steady state absorption for the nanostructures (c) and (d). The maxima indicate the positions of the lowest energetic allowed optical transitions and show, that the increase of the CdS clad from one to three monolayers leads only to a small redshift of the absorption features from 525 to 540 nm and from 625 to 640 nm, respectively. (Bottom) Fluorescence and excitation spectra of the QDQW nanoparticle CdS/HgS/$\{CdS\}_3$. The broad and weak emission of the colloidal solution can be enhanced by forming an inorganic capping layer of $Cd(OH)_2$ around the nanoparticles and the excitonic emission component also becomes more obvious. The optical excitation spectrum detected at 760 nm is identical for both samples and reproduces the absorption spectrum (top). All spectra were corrected for the sensitivity of the detection system or the emission characteristic of the XBO lamp, respectively.

rivatives of the absorption spectra (c) and (d), given in the inset of Fig. 1 (top), show that the optical transitions of the QDQW were only slightly redshifted (20 nm), by increasing the CdS clad. Also the derivatives allow us to determine the energetic positions of the two strongest optical transitions in the HgS well (below the band gap of the CdS core at 465 nm) at about 640 and 525 nm.

The emission spectrum at room temperature of the CdS/HgS/$\{CdS\}_3$ QDQW colloidal solution is shown in Fig. 1 (bottom). The emission band is broad and unstructured and extends from 650 nm to lower energies. Adding Cd^{2+} ions to the colloidal solution and increasing the pH value to 10.0 by adding drop by drop 0.1 M NaOH solution a layer of $Cd(OH)_2$ can be grown on the CdS surface. This leads to an increase in the fluorescence quantum yield as well as a more pronounced excitonic band gap emission component. This has been shown by other groups.[19,20] The fluorescence spectrum of this QDQW nanoparticle, denoted as CdS/HgS/$\{CdS\}_3$/$Cd(OH)_2$, is also shown in Fig. 1 (bottom). The excitonic emission has its maximum at 730 nm, which is in agreement with that reported by other groups.[19,23] The excitation spectrum probed at 760 nm is identical for both QDQW's and is given in Fig. 1 (bottom). The excitation spectrum is similar to the absorption spectrum of the QDQW, which shows that the absorbing and emitting species in the colloidal solution are identical. Furthermore, it suggests the absence of different types of high-energy nonradiative relaxation processes that do not lead to the electrons and holes giving rise to the observed emission.

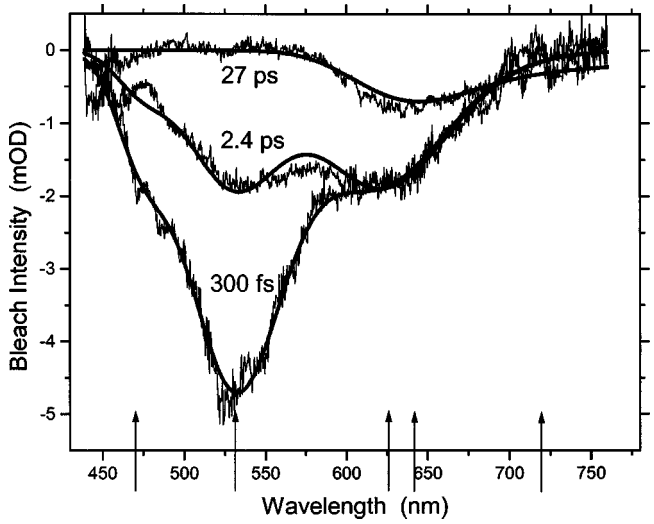

FIG. 2. Transient absorption spectra of a film of CdS/HgS/$\{CdS\}_3$ nanoparticles on a CaF_2 substrate at room temperature for different delay times between pump (400 nm) and probe pulse. The solid lines show the fit of the spectra to five Gaussians at 470, 530, 625, 640, and 720 nm. By comparison of these negative signals with the steady state absorption and emission (Fig. 1) the signal at 720 nm is identified with stimulated emission and the other four signals with bleach.

B. Femtosecond transient spectra

The room-temperature femtosecond time-resolved transient absorption spectra of the CdS/HgS/$\{CdS\}_3$ film on a CaF_2 substrate at different delay times between pump and probe pulse are shown in Fig. 2. The sample was excited at 400 nm, where the film has an absorbance of 1 OD. The transient absorption spectra show several negative bleach bands over the whole visible range and a very weak stimulated emission signal at longer wavelength where no ground state absorption can be observed. An energy diffusion with a faster relaxation of the higher-energy states can clearly be

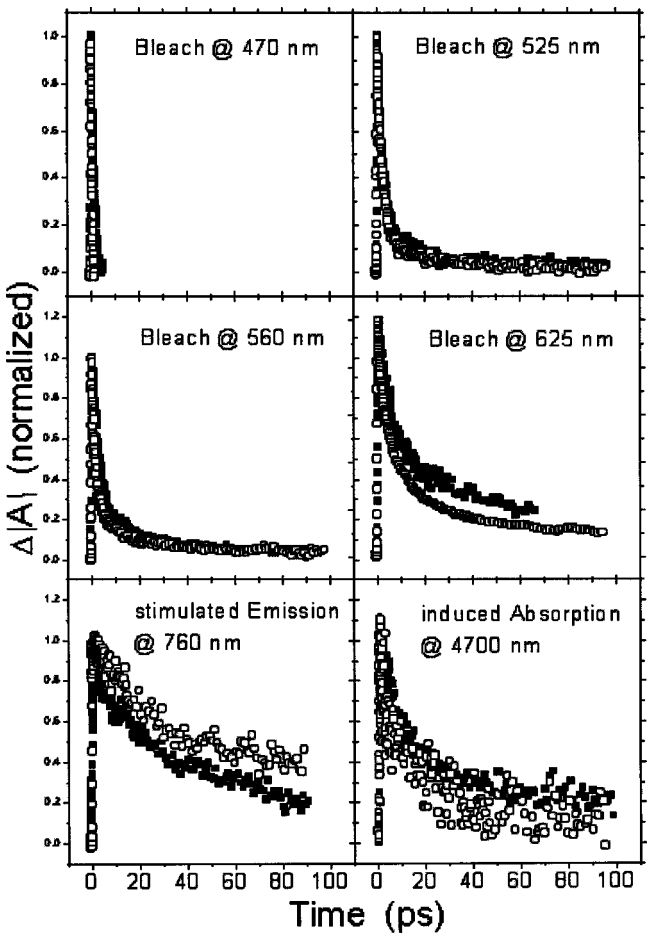

FIG. 3. Decay of the transient absorption signals of the QDQW nanoparticle CdS/HgS/$\{CdS\}_3$ after optical excitation at 400 nm (solid squares) and 650 nm (open circles). The bleach was probed at 470 nm (1 ps), 525 nm (1.5 ps/40 ps), 560 nm (3.7 ps/50 ps), and 625 nm (6.7 ps/90 ps), the stimulated emission was probed at 760 nm (55 ps) and the induced absorption was probed with an IR pulse at 4.7 μm (7.0 ps/110 ps). The decay times for 400 nm excitation are given in parentheses. The decay dynamics of all these signals is not noticeably changed after excitation at 650 nm directly into the HgS well. However, the rise times change drastically as shown in the next figures. (Note that for clarity all traces are shown as positive signals.)

observed. The positions of the bleach bands were determined by a simultaneous fit of the three spectra to 5 G curves. Their maxima are indicated by arrows (470, 530, 625, 640, and 720 nm). The first four bands are assigned to a bleach signal and the weak band at 720 nm to stimulated emission. This was done by comparing the energy positions of the negative transient absorption to the steady-state absorption and emission spectra in Fig. 1 consistent with previous reports.[24,27]

C. Femtosecond kinetics

In Fig. 3 the decay of the bleach signal at 470, 525, 560, and 625 nm, the stimulated emission signal at 760 nm, and the induced absorption signal at 4.7 μm after excitation at 400 nm (closed squares, excitation of the CdS core) and 650 nm (open circles, excitation of the HgS well) are shown for

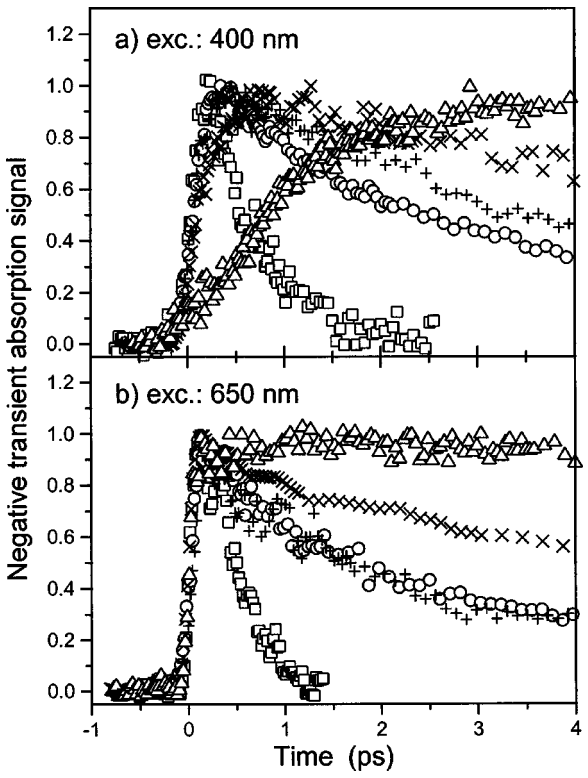

FIG. 4. The rise of the transient absorption signals at 470 nm (squares), 525 nm (circles), 560 nm (+), 625 nm (×), and 760 nm (triangles) of the QDQW nanoparticle CdS/HgS/$\{CdS\}_3$ after excitation with different wavelengths is shown. (a) Excitation at 400 nm (excitation at 266 nm leads to an identical rise behavior). The four bleach signals have rise times between 200 and 300 fs while the stimulated emission signal at 760 nm rises with 1.5 ps. (b) Excitation at 650 nm (excitation at 580 nm leads to an identical rise behavior). The four bleach signals and the stimulated emission signal rises faster than the pump pulse, therefore only an upper limit of 50 fs for the rise time can be given.

the CdS/HgS/$\{CdS\}_3$ nanoparticles. The higher energetic bleach bands decay faster indicating a relaxation of the excited electrons and holes to the bottom of the conduction band and the top of the valence band, respectively. The dynamics of the bleach at 625 nm, the stimulated emission signal at 760 nm, and the induced absorption signal at 4.7 μm are very similar suggesting that the decay of the same state is monitored. Also, only small differences between the bleach decays after excitation into the CdS core or the HgS well are seen. Mainly the relative amplitude ratio between a fast (sub 10 ps) and a longer (>10 ps) component is different. (The decay times after 400 nm excitation are given in the figure caption of Fig. 3.)

The rise times of the five signals as a function of the excitation wavelength is shown in Fig. 4. The rise times of the five signals after excitation at 400 nm is shown in Fig. 4(a). All four bleach signals have rise times between 200 and 300 fs, whereas the stimulated emission signal rises in 1.5 ps. Excitation at 266 nm (not shown here) gives the same values.

After optical excitation directly in HgS well states at 650 nm (and 580 nm, not shown, here) the rise of the bleach and stimulated emission signals, shown in Fig. 4(b), is not re-

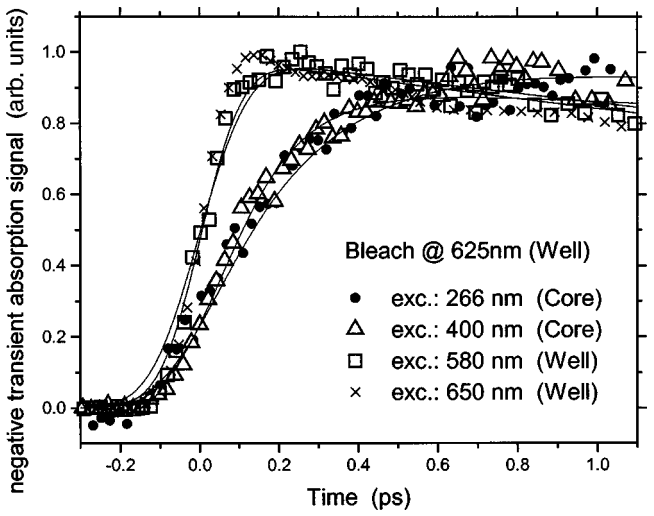

FIG. 5. The rise of the bleach signal observed at 625 nm of the QDQW nanoparticle CdS/HgS/$\{CdS\}_3$ after excitation with the wavelengths 266, 400, 580, and 650 nm is shown. For the excitation at 266 and 400 nm a rise time of 200–300 fs is observed. The rise of the signal after excitation at 580 and 650 nm is limited by the width of the pump pulse (100 fs).

solved from the pulse width of the pump and probe pulses (100 fs). Therefore, due to the resolution of the optical delay line (21 fs) and the pulse width (100 fs) only an upper limit of the rise times of about <50 fs can be estimated. A comparison of the rise times for the bleach signal at 625 nm after excitation at 266, 400, 580, and 650 nm is shown in Fig. 5.

In order to investigate intraband transitions in the CdS/HgS/$\{CdS\}_3$ QDQW system we excited optically an electron hole pair and probed the induced charge carrier transient absorption by an IR probe pulse at 4.7 μm well below the band gap absorption. The kinetic traces of the positive transient absorption signal for several excitation wavelengths (266, 400, 580, 650 nm) are shown in Fig. 6. The decay of the induced transient absorption was plotted in Fig. 3. The dependence of rise times of the induced absorption on the excitation wavelength shows a similar behavior to that of the bleach rise times (Figs. 4 and 5). Excitation of the sample at 580 and 650 nm leads to a rise of the induced absorption signal, which is within the duration of the pump and probe pulses (100 fs), whereas for excitation at 266 and 400 nm gives a rise time of the induced absorption signal of 250 and 150 fs, respectively.

IV. DISCUSSION

The transient absorption spectra (Fig. 2) of the QDQW system CdS/HgS/$\{CdS\}_3$ can be described by the superposition of five bands: four bleach bands at 470, 530, 625, and 640 nm and a weak stimulated emission signal at 720 nm. This is in very good agreement with the observed maxima of the second derivative of the steady state absorption spectrum (Fig. 1), from which the position of the two optically allowed transitions at about 640 and 525 nm could be resolved. The excitonic fluorescence of the sample (Fig. 1) with a maximum at 730 nm is also in good agreement with the weak

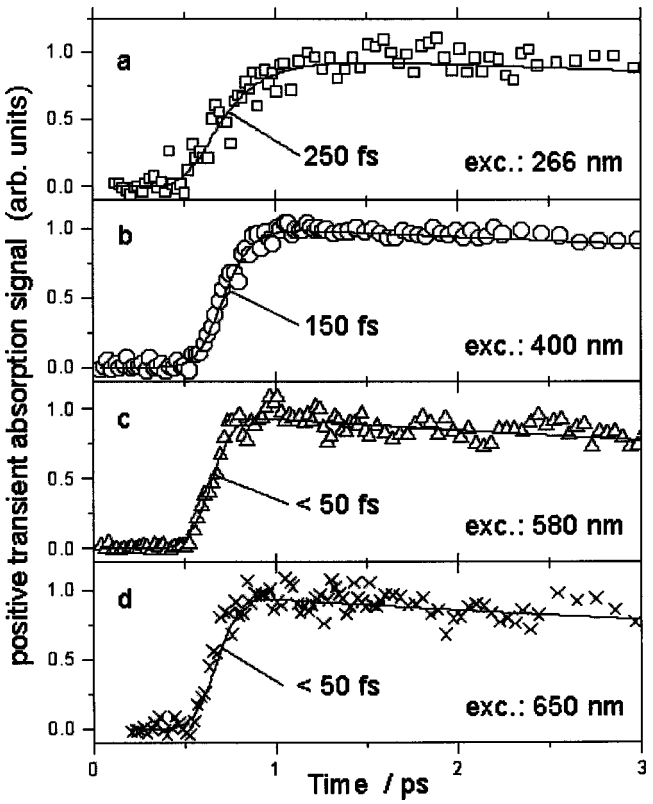

FIG. 6. The rise of the transient induced absorption signal monitored at 4.7 μm of the QDQW nanoparticle CdS/HgS/$\{CdS\}_3$ after excitation with different wavelengths is shown. (a) Excitation at 266 nm (rise time: 250 fs). (b) Excitation at 400 nm (rise time: 150 fs). (c) Excitation at 580 nm (rise time: <50 fs). (d) Excitation at 650 nm (rise time: <50 fs). The rise of the signals (c) and (d) is limited by the width of the pump pulse (100 fs) and only an upper limit of 50 fs for the rise time can be given.

stimulated emission band found at 720 nm in the transient absorption spectra. The assignment of the signal at 720 nm (and also at longer wavelength where we were also able to observe a increased differential transmission with our more sensitive single wavelength lock-in detection setup) is consistent with a previous assignment made by Yeh *et al.*[24] Furthermore, the positions of the bleach bands are also in good agreement with calculations by Jaskolski and Bryant[29] and allow an assignment of the transitions to $1S\text{-}1S_{3/2}$ (720 nm), $1P\text{-}1P_{3/2}$ (640 nm), $1P\text{-}1P_{1/2}$ (625 nm), and $1S\text{-}2S_{3/2}$ (530 nm). Our observed higher energetic allowed transitions have not yet been calculated.

The decay times of the bleach bands especially at the lowest optical transitions at 720 nm ($1S\text{-}1S_{3/2}$) and 640 nm ($1P\text{-}1P_{3/2}$) involving the $1P$ and $1S$ electrons in the range of tens of picoseconds is explained by the trapping of the electron and hole in shallow and deep traps. The population of the (unexcited) ground state occurs much later. From time-resolved fluorescence measurements[20] it is known that the radiative recombination of electron and hole is much slower and extends from the nanosecond to the microsecond range. The decay of the higher energy states is faster and consistent with the spectral diffusion seen in the transient absorption spectra shown in Fig. 2. The faster bleach decay

at shorter wavelength can be explained by the independent relaxation of the electrons and holes within the quantized energy levels. According to the state filling model[32] the bleach of an optical transition can be caused by either the occupation of a previously (before excitation) empty level by an electron or by the absence of an electron (presence of a hole). Since the relaxation of the electron and hole can be treated independently in the strong confinement region the bleach decay of a certain transition can be caused by either charge carrier which therefore means that the bleach rise time of a lower lying level is not necessarily directly correlated to the decay of a higher energetic transition. At the same time trapping of the charge carriers from higher energy states would also be possible and explain the spectral diffusion.

That both charge carriers are responsible for the observed bleach bands in this QDQW nanoparticle system is nicely demonstrated by the fact that excitation into the HgS well states leads to very similar bleach dynamics as shown in Fig. 3. In particular, even though excitation is carried out at low energies (650 nm) all of the higher energy states are also bleached which confirms that it takes only one of the charge carriers to be excited in order to cause the bleaching of several transitions. Furthermore, the hole plays a much more important role in this system than for example in CdSe nanoparticles for which the bleach is mainly dominated by the occupation of electronic levels.[32] This is due to the high density of hole states in CdSe nanoparticles. With only one monolayer of HgS the separation of the hole states is much larger (see also below the discussion of the mid-IR absorption) and is actually comparable to the energy separation of electronic states in CdSe.

The rise times of the four bleach signals and the stimulated emission signal after direct excitation in HgS well states (at 580 and 650 nm) are faster than the pulse width of the laser used. Therefore an upper limit of 50 fs was estimated (see Figs. 4 and 5). On the other hand, after optical excitation in states, which are energetically higher than the HgS well and with their wave functions extended over the whole nanostructure, a rise time for the bleach signals in the HgS well of 200–300 fs was found. This time can therefore be assigned to the localization time of one of the charge carriers into the HgS well because only one of them, electron or hole, is needed to lead to the observed bleach signal. On the other hand, the rise time of the stimulated emission signal is much slower with 1.5 ps after excitation of the CdS core states (at 400 and 266 nm). This can be explained by the localization time of the charge carrier with the slower localization probability. For the stimulated emission process, both charge carriers are needed to be present in the HgS well in order to recombine radiatively. The charge carrier with the slower localization time determines the rise of that signal.

While visible bleach features in semiconductor nanostructures are complicated because of the contribution of the electron and hole to the observed signal, using infrared probe light with energies below the bandgap energy allows one to selectively probe transition between quantized electron and hole levels. Since the energy separation between electron and hole levels is usually very different because of their different effective masses a more detailed assignment is possible. We found an induced absorption signal of the QDQW structure at a probe wavelength of 4.7 μm. The induced absorption shows the same biexponential decay behavior as the bleach signal at 625 nm (see Fig. 3). The rise time of the signal after direct excitation of HgS well states (at 580 and 650 nm) is with $<$50 fs similar to the rise time of the visible bleach signals. After excitation of CdS core states (at 400 and 266 nm) a rise time of 150–250 fs was found, again similar to the rise times of the bleach bands for the same excitation wavelength. It can therefore be concluded that the induced absorption signal has a similar rise and decay behavior as the bleach signal of the HgS well transitions, which indicates that the same charge carrier is involved for both signals. The reason why the rise of the transient absorption signal in the midinfrared region is slightly faster than the bleach rise times is the fact that even before the crossing of the CdS/HgS interface intraband transition within the energy levels of the CdS core could be probed. This would lead to a faster rise time and could explain the slight difference between the bleach rise times and the induced IR absorption.

Theoretical calculations[29] for the QDQW system have been performed which give an energy difference of about 0.28 eV between the lowest hole state $1P_{3/2}$ and the $1S_{3/2}$ state. This corresponds to a transition wavelength of 4.4 μm in good agreement with our observation wavelength of 4.7 μm considering the broadening of the transition due to the sample size distribution. According to the same theoretical calculations the energy difference between the two lowest electron states in the conduction band is much larger with 0.37 eV corresponding to a transition wavelength of 3.3 μm. It can thus be concluded that the IR probe pulse at 4.7 μm does not interact with the electrons in the conduction band. Therefore, we assign the bleach rise time of 200–300 fs to the localization time of the hole, not the electron, in the HgS well. The rise time of 1.5 ps then corresponds to the localization time of the electron from the CdS core into the HgS well states.

The large difference in the transfer time of the electron and hole across the CdS/HgS interface can be explained by the effective mass of the electron and hole in the core and well. The effective mass of the hole in the valence bands of CdS and HgS are quite similar,[29] while the effective mass of the electron in the conduction bands in the two materials is different. This makes it easier for the hole to cross the interface than the electron. However, such an explanation might not be justified since the HgS well consists only of one monolayer and therefore does not even have a full unit cell. Using a molecular approach to this problem one can argue that the much faster transfer rate of the hole compared to the electron across the interface is due to a charge resonant transfer between two sulfur ions for the hole while the electron has to be transferred from a cadmium to mercury ion. If the ground state of the CdS and HgS can be thought of having the $M^{2+}S^{2-}$ ionic structure then the excited state can be approximated by $M^{1+}S^{1-}$. This means that the excitation is considered as an electron transfer from S^{2-} to M^{2+} and a hole transfer from M^{2+} to S^{2-}. In this particular case for the CdS/HgS/CdS QDQW nanoparticle system the localization

of the charge carriers in the HgS well after excitation of the CdS core would then involve the transfer of the charge carriers from the $(Cd^{1+}S^{1-})^*$ excited state to the ground state of the HgS $(Hg^{2+}S^{2-})_0$. The hole transfers from S^{1-} of the $(Cd^{1+}S^{1-})^*$ to the S^{2-} of the $(Hg^{2+}S^{2-})_0$ and the electron transfers from Cd^{1+} of CdS to the Hg^{2+} of HgS according to

$$(Cd^{1+}S^{1-})^* + (Hg^{2+}S^{2-})_0 \rightarrow (Cd^{2+}S^{2-})_0 + (Hg^{1+}S^{1-})^*.$$

Since the hole transfer process is a charge resonance process between two sulfur ions it is expected to be faster than the electron transfer between different types of ions. The latter would need to be assisted by phonon processes, which reduce the transfer rate. In the molecular electron transfer language, the Franck-Condon factors are therefore expected to be much larger for the hole transfer compared to the electron transfer. Furthermore, the density of hole states in the valence band is much higher due to the degeneracy of the *p* orbitals of the sulfur ions. As the rate of the observed charge transfer processes is related to both the Franck-Condon factors as well as the density of states, one would expect a faster hole transfer in agreement with our experimental results.

V. CONCLUSION

We presented in this work the results on steady state and femtosecond time-resolved measurements on CdS/HgS/$\{CdS\}_3$ QDQW nanoparticles. By comparing the bleach, stimulated emission and induced absorption signals found in the transient measurements as a function of the excitation energy, we determined the localization times of electrons and holes in the HgS well, separately. We found that the electron localization time in the HgS well after CdS core excitation is 1.5 ps while that of the hole is ~150 fs. This large difference in the observed dynamics of the electron and hole in crossing the CdS/HgS interface was discussed in terms of a resonant charge transfer process of the hole between the sulfur atoms in the CdS core and the sulfur atoms in the HgS well. The energies of the observed signals are furthermore in very good agreement with theoretical calculations by Jaskolski and Bryant and higher energy states not yet calculated were determined.

ACKNOWLEDGMENTS

This work was supported by the Office of Naval Research (ONR Grant No. CHE-9727633). M. Braun wishes to thank the Alexander von Humboldt Foundation for financial support.

*Present address: Lehrstuhl für BioMolekulare Optik, Ludwig-Maximilians-Universität München, D-80538 München, Germany.
†Present address: Chemistry Department, Case Western Reserve University, Cleveland, OH 44106.
‡Author to whom correspondence should be addressed.

[1] Z. I. Alferov and N. N. Ledentsov, Proc. SPIE **3625**, 2 (1999).
[2] B. Zhao and A. Yariv, Semicond. Lasers **1**, 1 (1999).
[3] E. Kapon, Semicond. Lasers **1**, 291 (1999).
[4] H. Sakaki, Phys. Status Solidi B **215**, 291 (1999).
[5] C. Weisbuch, H. Benisty, and R. Houdre, J. Lumin. **85**, 271 (2000).
[6] O. Wada, Opt. Quantum Electron. **32**, 453 (2000).
[7] A. Ramdane and A. Ougazzaden, Mater. Sci. Eng. B **74**, 66 (2000).
[8] C. B. Murray, D. J. Norris, and M. G. Bawendi, J. Am. Chem. Soc. **115**, 8706 (1993).
[9] M. A. Hines and P. Guyot-Sionnest, J. Phys. Chem. **100**, 468 (1996).
[10] C. B. Murray, C. R. Kagan, and M. G. Bawendi, Annu. Rev. Mater. Sci. **30**, 545 (2000).
[11] R. Rossetti, J. L. Ellison, J. M. Gibson, and L. E. Brus, J. Chem. Phys. **80**, 4464 (1984).
[12] L. E. Brus, in *Nanophase Materials: Synthesis—Properties—Applications*, edited by S. Y. Nof, NATO Adv. Study Inst. Ser., Ser. E Vol. **260** (Kluwer, Dordrecht, 1994), p. 433.
[13] X. Peng, M. C. Schlamp, A. V. Kadavanich, and A. P. Alivisatos, J. Am. Chem. Soc. **119**, 7019 (1997).
[14] M. Gao, S. Kirstein, A. L. Rogach, H. Weller, and H. Mohwald, Adv. Sci. Technol. (Faenza, Italy) **27**, 347 (1999).
[15] B. Winkler, L. Dai, and A. W.-H. Mau, J. Mater. Sci. Lett. **18**, 1539 (1999).
[16] M. Bruchez, M. Moronne, P. Gin, S. Weiss, and A. P. Alivisatos, Science **281**, 2013 (1998).
[17] W. C. W. Chan and S. Nie, Science **281**, 2016 (1998).
[18] A. Eychmüller, A. Mews, and H. Weller, Chem. Phys. Lett. **208**, 59 (1993).
[19] A. Mews, A. Eychmüller, M. Giersig, D. Schooss, and H. Weller, J. Phys. Chem. **98**, 934 (1994).
[20] A. Mews and A. Eychmüller, Ber. Bunsenges. Phys. Chem. **102**, 1343 (1998).
[21] F. Koberling, A. Mews, and T. Basché, Phys. Rev. B **60**, 1921 (1999).
[22] A. Mews, A. V. Kadavanich, U. Banin, and A. P. Alivisatos, Phys. Rev. B **53**, R13 242 (1996).
[23] E. Lifshitz, H. Porteanu, A. Glozman, H. Weller, M. Pflughoefft, and A. Eychmüller, J. Phys. Chem. B **103**, 6870 (1999).
[24] A. T. Yeh, G. Cerullo, U. Banin, A. Mews, A. P. Alivisatos, and C. V. Shank, Phys. Rev. B **59**, 4973 (1999).
[25] V. F. Kamalov, R. Little, S. L. Logunov, and M. A. El-Sayed, J. Phys. Chem. **100**, 6381 (1996).
[26] R. B. Little, C. Burda, S. Link, S. Logunov, and M. A. El-Sayed, J. Phys. Chem. A **102**, 6581 (1998).
[27] M. Braun, C. Burda, M. Mohamed, and M. A. El-Sayed, Phys. Rev. B **64**, 035317 (2001).
[28] G. Bryant, Phys. Rev. B **52**, R16 997 (1995).
[29] W. Jaskólski and G. Bryant, Phys. Rev. B **57**, R4237 (1998).
[30] K. Chang and J.-B. Xia, Phys. Rev. B **57**, 9780 (1998).
[31] M. Braun, S. Link, C. Burda, and M. A. El-Sayed, Chem. Phys. Lett. **361**, 446 (2002).
[32] V. I. Klimov, in *Handbook of Nanostructured Materials and Nanotechnology*, edited by H. S. Nalwa (Academic, San Diego, 2000), Vol. 4.